Formation Mechanisms of Mound-Like Multiscale Surface Structures by Femtosecond Laser Surface Processing on Amorphous & Polycrystalline $Ni_{60}Nb_{40}$

Edwin Peng[1], Alfred Tsubaki[2], Craig Zuhlke[2], Ryan Bell[2], Meiyu Wang[1], Dennis R. Alexander[2], George Gogos[1], & Jeffrey E. Shield[1]

[1]Department of Mechanical & Materials Engineering [2]Department of Electrical Engineering

CEFS Center for Electro-Optics & Functionalized Surfaces

NCMN Nebraska Center for Materials and Nanoscience, University of Nebraska

Why FLSP?

Promising Surface Functionalization Technique

- Femtosecond Laser Surface Processing (FLSP)
- Utilize high power, femtosecond (10^{-15} s) laser pulses
- Produce self-organized, multiscale surface micro/nanostructures
- Diverse range of applicable substrates: semiconductors, metals, polymers, & composites

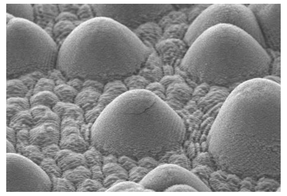

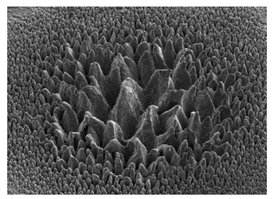

Properties & Applications

- Electrical & optical properties: solar cells, photodetectors
- Special wetting properties: self-cleaning surfaces, biomedical implants, heat transfer, drag reduction, anti-icing

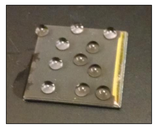

Ni60Nb40 Substrate

Why $Ni_{60}Nb_{40}$?

- Well-characterized, easy metallic glass-forming alloy
- Previous "laser vitrification" demonstrated amorphous phase formation at heat-affected zone (HAZE)

Synthesis

- All synthesis in inert Ar atmosphere
- Arc melt pure Ni (99.995+%) & Nb (99.95+%)
- melt-spin into amorphous $Ni_{60}Nb_{40}$ ribbons (150 µm thick, 4 mm wide)
- annealed into polycrystalline $Ni_{60}Nb_{40}$ ribbons at 1373 K for 20 hrs

Characterization

- Bruker-AXS D8 X-Ray Diffractometer: phase identification w/ X-ray diffraction (XRD)
- FEI Helios NanoLab 660: microstructure imaging w/ ion-induced secondary electron (ISE) imaging & compositional analysis w/ energy dispersive x-ray spectroscopy (EDS)

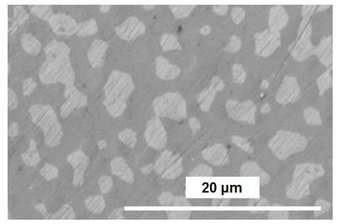

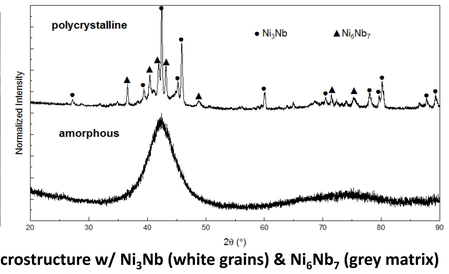

Left: ISE image of polycrystalline $Ni_{60}Nb_{40}$ microstructure w/ Ni_3Nb (white grains) & Ni_6Nb_7 (grey matrix)
Right: XRD pattern of polycrystalline and amorphous $Ni_{60}Nb_{40}$

Ablation Threshold

Spectra-Physics Spitfire Laser System

- Ti:sapphire
- 80 fs, 1 mJ maximum pulse energy
- Melles Griot Nanomotion II 3-axis translation stage

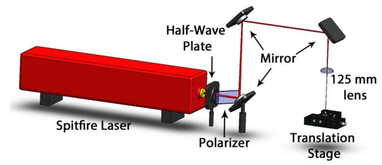

Ablation Threshold Testing

- 100 50 fs pulses from 50 to 700 mW power
- Keyence VK-X: measure ablated area w/ 3D laser scanning confocal microscope (3DLSCM)
- No significant difference between ablation threshold of amorphous vs polycrystalline $Ni_{60}Nb_{40}$ substrates

	Amorphous	Polycrystalline
Spot Radius (µm)	104 ± 2	102 ± 3
Threshold Fluence (J cm-2)	0.100 ± 0.004	0.102 ± 0.007

FLSP Mounds Formation

FLSP Raster

- 1x1 mm raster
- Gaussian profile
- BSG mounds
  - Laser fluence: 2.14 J cm^{-2}
  - 625 laser pulses
  - Translation speed: 3 mm s^{-1}
  - Pitch: 15 µm
- ASG mounds
  - Laser fluence: 6.10 J cm^{-2}
  - 175 laser pulses
  - Translation speed: 4.5 mm s^{-1}
  - Pitch: 15 µm

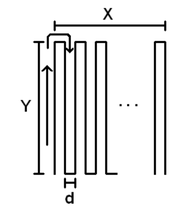

Objectives

Why?

- Below-Surface Growth (BSG) & Above-Surface Growth (ASG) mounds on metals important for their potential applications
- BSG & ASG mound formation on Ni 200/201 previously studied using stop motion Scanning Electron Microscopy (SEM) imaging
- Need physical evidence of formation models

How?

- Obtain evidence of mound growth processes by examining underlying microstructure
- Utilize dual beam SEM-Focused Ion Beam (FIB) instrument to cross section BSG & ASG mounds
- Easy glass-forming alloy as target substrate to visualize any rapid solidification processes

BSG- vs ASG-Mound Formation Models

Mound-Like Multiscale Structures

- FLSP forms two distinct mound-like structures on metals
- Below Surface Growth (BSG) Mounds
  - Mounds with peaks *below* original substrate surface
  - Occur when laser fluence >> ablation threshold
  - Growth theorized to be dominated by preferential valley ablation
- Above Surface Growth (ASG) Mounds
  - Mounds with peaks *above* original substrate surface
  - Occur at higher laser fluence, lower # laser pulses than BSG-mounds
  - Growth theorized to be dominated by preferential valley ablation and redeposition due to hydrodynamical fluid flow
  - May be some redeposition from cloud of ablated substrate material

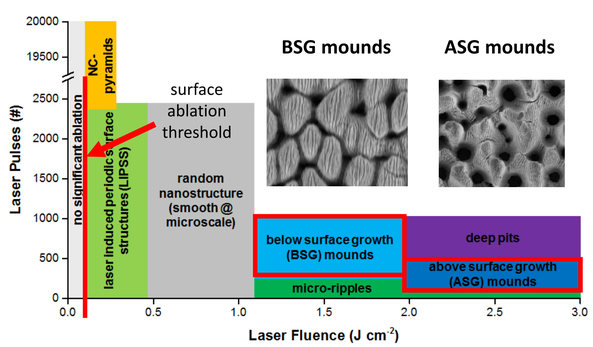

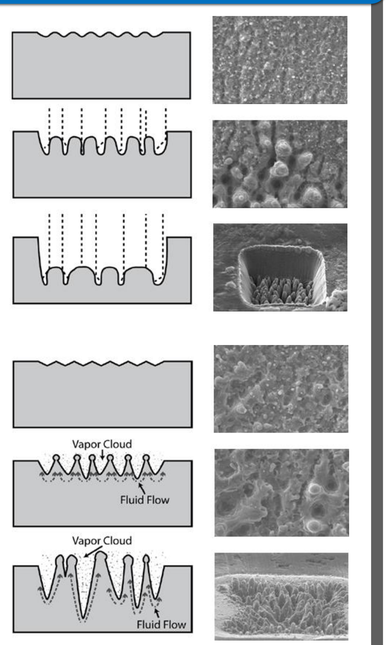

Right: Types of micro/nanostructures obtained by FLSP on Ni 200/201 surface
Top Left: formation model of BSG mounds
Bottom Left: formation model of ASG mounds

FLSP Mounds Results & Analysis

BSG Mounds

- BSG mounds produced on amorphous & polycrystalline substrates have same morphology (width & height)
- Cross section microstructure did change from original, pre-FLSP $Ni_{60}Nb_{40}$ substrates
- Evidence that primary BSG mound formation process was preferential valley ablation

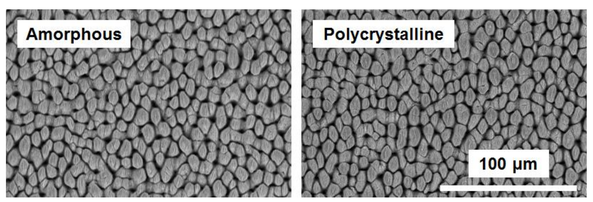

	Amorphous	Polycrystalline
Peak to peak distance (µm)	7.7 ± 0.2	7.9 ± 0.1
R_Z (µm)	15.6 ± 1.1	0.102 ± 0.007
R_{RMS} (µm)	3.0 ± 0.2	2.8 ± 0.2

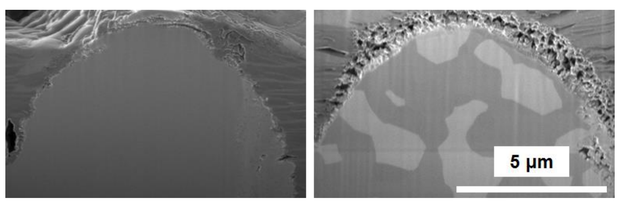

Top: ISE image of BSG mounds on amorphous & polycrystalline $Ni_{60}Nb_{40}$ substrates
Bottom Left: ISE image of typical cross section BSG mound on amorphous
Bottom Right: ISE image of typical cross section BSG mound on polycrystalline

ASG Mounds

- BSG mounds produced on amorphous substrates larger (width & height) than those on polycrystalline substrates
- Likely due to thicker fluid flow layer as amorphous substrate has lower thermal conductivity
- Cross section microstructure show additional, rapidly solidified fluid flow layer on top
- Confirm this fluid flow layer was amorphous $Ni_{60}Nb_{40}$ w/ selected area electron diffraction (SAED)

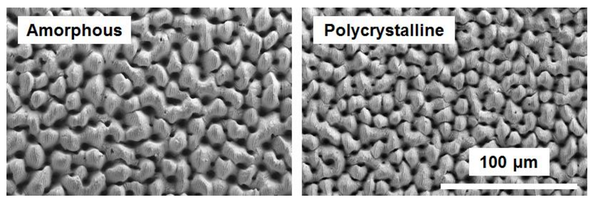

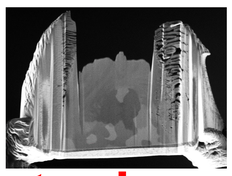

	Amorphous	Polycrystalline
Peak to peak distance (µm)	15.1 ± 0.2	13.3 ± 1.6
R_Z (µm)	28.8 ± 2.4	20.2 ± 2.0
R_{RMS} (µm)	6.0 ± 0.7	4.1 ± 0.5

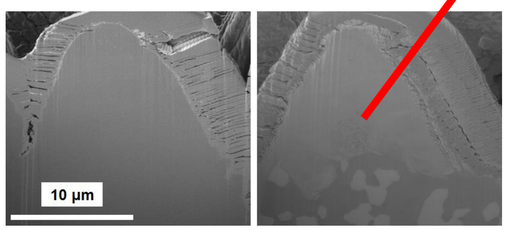

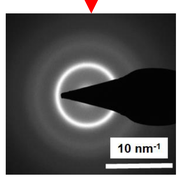

Top: ISE image of ASG mounds on amorphous & polycrystalline $Ni_{60}Nb_{40}$ substrates
Bottom Left: ISE image of typical cross section ASG mound on amorphous
Bottom Center: ISE image of typical cross section ASG mound on polycrystalline
Right: TEM liftout sample & SAED pattern of the solidified fluid flow layer

References

1. E. Peng, A. Tsubaki, C. A. Zuhlke, M. Wang, R. Bell, M. J. Lucis, T. P. Anderson, D. R. Alexander, G. Gogos and J. E. Shield, *Applied Physics Letters*, 2016, **108**, 031602.
2. C. A. Zuhlke, T. P. Anderson and D. R. Alexander, *Opt Express*, 2013, **21**, 8460-8473.
3. C. M. Kruse, T. Anderson, C. Wilson, C. Zuhlke, D. Alexander, G. Gogos and S. Ndao, *International Journal of Heat and Mass Transfer*, 2015, **82**, 109-116.
4. A. Y. Vorobyev and C. Guo, *Laser & Photonics Reviews*, 2013, **7**, 385-407.
5. G. Sepold and R. Becker, in *Science and Technology of the Undercooled Melt*, Springer, 1986, pp. 112-120.

Acknowledgements

Funding

- NASA EPSCoR Grant #NNX13AB17A
- Nebraska Research Initiative
- Nebraska Center for Energy Sciences Research (NCESR)

Research Facilities

- Nebraska Center for Materials and Nanoscience (NCMN)
- NanoEngineering Research Facility (NERF)